THE JOURNAL OF PHYSICAL CHEMISTRY B

Article

pubs.acs.org/JPCB

Resonance Energy Transfer in DNA Duplexes Labeled with Localized Dyes

Paul D. Cunningham,*[,†] Ani Khachatrian,[†,‡] Susan Buckhout-White,[†,§] Jeffrey R. Deschamps,[†] Ellen R. Goldman,[†] Igor L. Medintz,[†] and Joseph S. Melinger*[,†]

[†]U.S. Naval Research Laboratory, 4555 Overlook Avenue SW, Washington, DC 20375, United States

[‡]Sotera Defense, 430 National Business Parkway, Suite 100, Annapolis Junction, Maryland 20701, United States

[§]George Mason University, 10910 University Boulevard, MS 4E3, Manassas, Virginia 20110, United States

Supporting Information

ABSTRACT: The growing maturity of DNA-based architectures has raised considerable interest in applying them to create photoactive light harvesting and sensing devices. Toward optimizing efficiency in such structures, resonant energy transfer was systematically examined in a series of dye-labeled DNA duplexes where donor−acceptor separation was incrementally changed from 0 to 16 base pairs. Cyanine dyes were localized on the DNA using double phosphoramidite attachment chemistry. Steady state spectroscopy, single-pair fluorescence, time-resolved fluorescence, and ultrafast two-color pump−probe methods were utilized to examine the energy transfer processes. Energy transfer rates were found to be more sensitive to the distance between the Cy3 donor and Cy5 acceptor dye molecules than efficiency measurements. Picosecond energy transfer and near-unity efficiencies were observed for the closest separations. Comparison between our measurements and the predictions of Förster theory based on structural modeling of the dye-labeled DNA duplex suggest that the double phosphoramidite linkage leads to a distribution of intercalated and nonintercalated dye orientations. Deviations from the predictions of Förster theory point to a failure of the point dipole approximation for separations of less than 10 base pairs. Interactions between the dyes that alter their optical properties and violate the weak-coupling assumption of Förster theory were observed for separations of less than four base pairs, suggesting the removal of nucleobases causes DNA deformation and leads to enhanced dye−dye interaction.

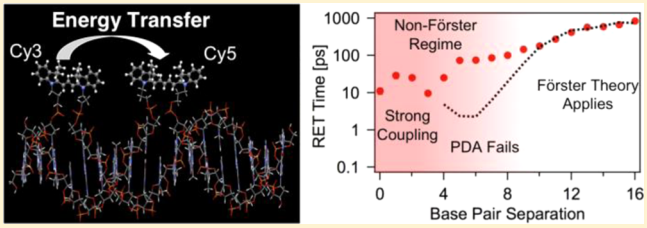

INTRODUCTION

Photosynthetic systems harvest light through chromophore−protein complexes and then funnel electronic excitations to a reaction center. The funneling is enabled via efficient nonradiative resonance energy transfer (RET) through an array of chromophores with well-defined positions and relative orientation.[1] The creation of synthetic light harvesting (LH) structures that mimic those found in nature is a challenging task. Optimizing synthetic LH structures requires well-organized chromophores and a detailed understanding of RET. Recently, DNA nanotechnology[2] has shown promise as a tool to construct LH structures ranging from relatively simple DNA duplexes[3−5] to more complex geometric shapes including hexagons,[6] bundles,[7] tetrahedrons,[8] and DNA origami.[9] In each case, the DNA serves as a scaffold to organize chromophores into specific patterns to produce directed RET.

The motivation for this study comes from our desire to develop design criteria to make efficient light harvesting antennae using a DNA scaffold. Consideration must be given to optimizing the chromophore−chromophore separation, transition dipole orientations, and the attachment chemistry of each chromophore onto the DNA duplex. In this work, we focus primarily on describing how the energy transfer efficiency depends on the donor−acceptor separation distance. While we intuitively expect the energy transfer efficiency to increase as the donor−acceptor pair is brought closer together, at what separation do we introduce other photophysical processes that compete with energy transfer? Further, over what range of chromophore separations does Förster theory describe the energy transfer rate and efficiency?

The DNA double helix provides the simplest means for creating a model system in which the RET process can be systematically studied over well-controlled donor−acceptor distances. To do this, we use the double phosphoramidite attachment chemistry that localizes cyanine dyes within the region of a specific base pair along the DNA duplex, see Figure 1, and therefore allows the donor−acceptor distance to be estimated with greater accuracy compared to flexible chromophore attachments. We anticipated that the double phosphoramidite attachment would also hold the transition dipole orientation fixed, but we conclude, as others[10] recently have, that the cyanine transition dipole is not highly oriented.

Received: June 30, 2014
Revised: November 10, 2014
Published: November 14, 2014

   dx.doi.org/10.1021/jp5065006 | J. Phys. Chem. B 2014, 118, 14555−14565

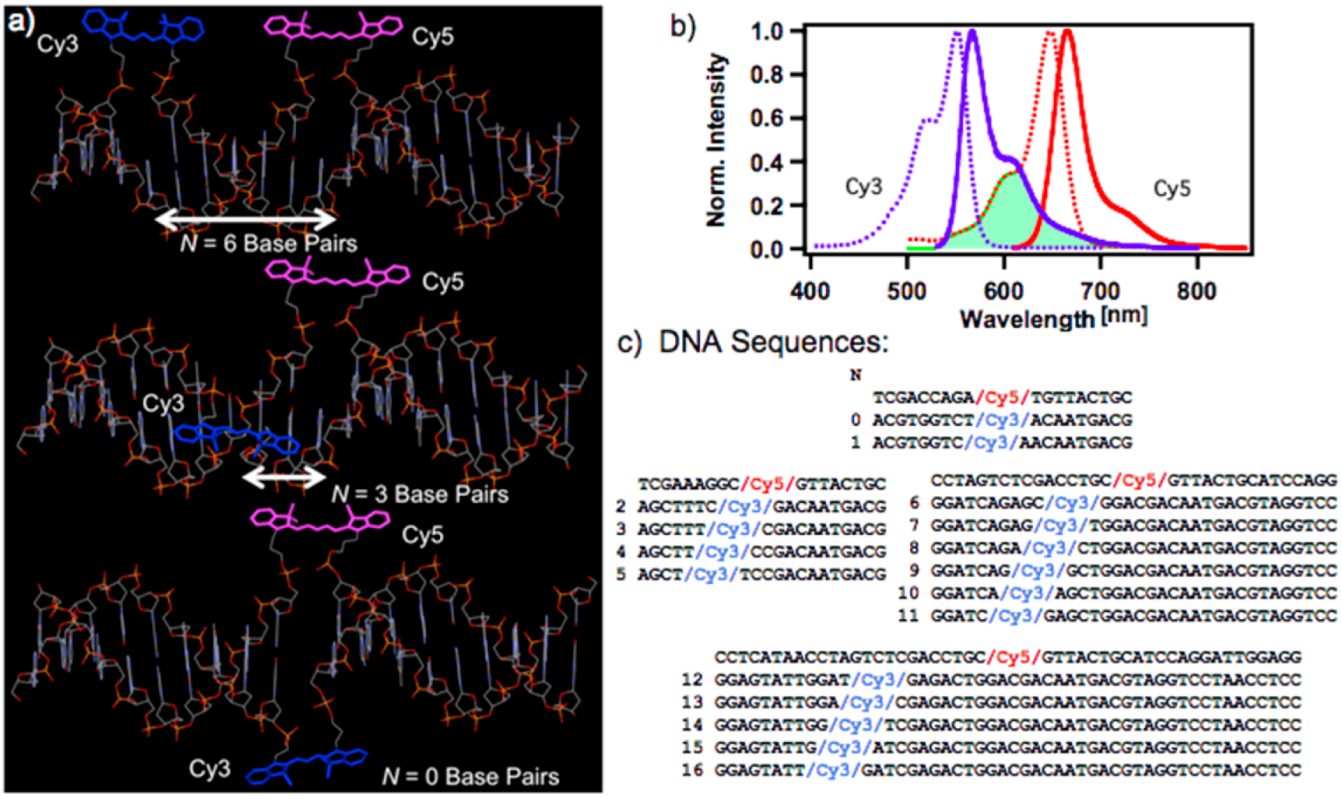

Figure 1. (a) Representative Cy3−Cy5-labeled DNA duplexes from the structural modeling described in Materials and Methods. The $N = 6$ strand has been truncated for ease of comparison. (b) Absorption (dotted) and fluorescence (solid) spectra of Cy3-only and Cy5-only labeled DNA duplexes. The spectral overlap region is shown (green). (c) DNA sequences for $N = 0$−16 base-pair separation dye-labeled DNA duplexes.

Even so, the DNA helix with localized dyes can be used to compare RET in regimes that include Förster type RET and non-Förster type RET, where the donor−acceptor coupling is no longer small and the point dipole approximation is questionable. A detailed understanding of RET within the scaffold provided by the DNA duplex will be important in order to optimize excitation funneling from RET in more complex DNA structures.

In the Förster limit, the electronic excitation is transferred from a donor chromophore to a resonant state in an acceptor chromophore via coupling between the two transition dipole moments. This process is often called Förster resonance energy transfer (FRET). FRET depends on the donor−acceptor separation (R), the donor fluorescence quantum yield (Q_D), the relative orientations of the transition dipole moments, and the Franck−Condon overlap, which is typically approximated by the spectral overlap integral ($J(\lambda)$) between donor emission spectrum and acceptor molar absorptivity spectrum. The FRET rate depends on the donor excited state lifetime, τ_D, via

$$k_{FRET} = \frac{1}{\tau_D}\left(\frac{R_0}{R}\right)^6 \tag{1}$$

where R_0, known as the Förster distance, is the donor−acceptor separation that corresponds to an energy transfer efficiency of 50%. The FRET efficiency is defined as

$$E = \frac{{R_0}^6}{{R_0}^6 + R^6} \tag{2}$$

This is a quantum efficiency, which ignores loss of energy due to thermalization of the chromophore excited states. Both the rate and efficiency are strongly dependent on the distance between the donor and acceptor. The Förster distance is given in units of angstroms by

$$R_0 = 9780[\kappa^2 n^{-4} Q_D J(\lambda)]^{1/6} \tag{3}$$

where $J(\lambda)$ is in units of $cm^3 \cdot M^{-1}$, n is the refractive index, and κ^2 is an orientation factor often taken to be 2/3, which implies a dynamic average of random dipole orientations. The overlap integral is calculated from the normalized donor fluorescence spectrum, $F_D(\lambda)$, and acceptor molar absorptivity spectrum, $\varepsilon_A(\lambda)$, as

$$J(\lambda) = \int_0^\infty F_D(\lambda)\lambda^4 \varepsilon_A(\lambda)\, d\lambda \tag{4}$$

While historically RET is observed through steady state ensemble efficiency measurements, single-particle ET measurements[11,12] discern subpopulations in heterogeneous ensembles allowing for RET to be used as a probe of nanoscale systems, e.g., protein folding.[13] Time-resolved measurements often yield complementary information to steady state measurements by providing direct access to the energy transfer dynamics instead of only the efficiency.

Synthetic light harvesting requires (quantum) energy transfer efficiencies larger than 90% per energy transfer step. Such highly efficient RET, in turn, requires sufficiently closely spaced fluorophores, $R \leq 0.69R_0$. In this regime RET is anticipated to proceed on the picosecond (or even sub-picosecond) time scale, so that characterization of the fastest RET dynamics will require ultrafast time resolution. To date, there have been few studies attempting to measure ultrafast RET in materials that use the DNA scaffold. Recently, Kato et al.[14] measured RET

dx.doi.org/10.1021/jp5065006 | J. Phys. Chem. B 2014, 118, 14555−14565

dynamics between fluorophores that have replaced base pairs on the DNA duplex. In that study the RET dynamics were measured as a function of donor−acceptor distance by time-resolved fluorescence using a streak camera. However, the instrument response was insufficient to resolve the fastest RET dynamics which occur at close donor−acceptor separation (~≤10 Å). In a different study, Xu et al.[15] used ultrafast pump−dump emission spectroscopy to measure picosecond time scale RET dynamics and transition dipole orientation dynamics in a hybrid polymer−dsDNA−chromophore system.

Here we explore the dependence of the RET rate and efficiency on the donor−acceptor separation between Cy3 and Cy5 dyes attached to DNA duplexes through a double phosphoramidite linkage. The RET efficiencies are quantified via single-pair FRET (spFRET), time-resolved fluorescence, and ultrafast pump−probe spectroscopy. The advantages of time-resolved spectroscopy, and specifically ultrafast pump−probe spectroscopy, are demonstrated. We find that, for small donor−acceptor separations, $N < 8$ base pairs (where N is the number of base pairs counted starting from the donor and ending on the acceptor; e.g., see Figure 1a), ultrafast spectroscopy is necessary to quantify the RET rates and to estimate the RET efficiencies. Deviations are observed from the predicted RET rates and efficiencies based on a structural model of the DNA duplexes for $N < 10$. The possible source of this discrepancy is discussed in terms of failure of the point dipole approximation. Interactions between the dyes are observed in the absorption spectrum for donor−acceptor separations of less than four base pairs and discussed in terms of the molecular exciton model.

MATERIALS AND METHODS

Cy3−Cy5-Labeled DNA Duplexes. Double-stranded DNA was assembled to accommodate controlled separation of the Cy3 donor and Cy5 acceptor fluorophores,[16] Figure 1a. The DNA oligos were designer synthetic sequences that were purchased from Integrated DNA Technologies (Coralville, IA, USA). All DNA sequences are listed in Figure 1c. The sequences were modified from the 48mer structures detailed in Wang and Seeman.[17] Both dyes were internally labeled and rigidly attached via two phosphoramidite linkers to reduce the uncertainty in position.[18] Originally, this attachment chemistry was also thought to provide a rigid attachment and thereby reduce uncertainty in dye orientation. However, very recent molecular dynamics simulations indicate the possibility of multiple dye orientations.[10] The position of Cy3 is varied to create a series where the separation between Cy3 and Cy5 covers $N = 0$−16 base pairs (bp).

For each DNA configuration, equimolar amounts of each oligo were mixed in 2.5 × phosphate buffered saline (PBS) to form a 20 μM stock solution. The DNA duplexes were assembled to a 2 μM concentration for a final volume of 1 mL in a 1.5 mL eppendorf tube. The tube was placed in a 95 °C thermal block for 5 min and allowed to cool slowly over an hour and a half until it reached 30 °C. Tubes were gently centrifuged and placed at 4 °C for at least several hours before measurements were taken. $MgCl_2$ was excluded due to the potentially deleterious effects high concentrations of such ions can have on dye fluorescence.[19] The use of high salt concentrations (such as 2.5 × PBS) to maintain DNA structures without $MgCl_2$ has been previously validated.[20]

Structural Modeling of DNA Duplexes. As a starting point for the discussions of experimental results presented later, we use a double-stranded DNA model that is constructed using *make-na*, a web-based utility (http://structure.usc.edu/make-na/server.html) that builds a three-dimensional (3-D) model from a linear DNA sequence using Nucleic Acid Builder.[21] Cy3, Cy5, and linker models were created using tools in UCSF Chimera (version 1.4.1).[22] Energy minimization was carried out in Chimera using built-in features including ANTECHAMBER (version 1.27) and the AM1-BCC method of calculating charges.[23] Based on these models, the separation between oxygen atoms that form the bridge to the phosphate esters range from 2.25 to 13.26 Å in Cy3 and from 4.85 to 15.52 Å in Cy5 while the oxygen−oxygen separation along the phosphate ester chain ranges from 6.35 to 7.20 Å. When bond angles and steric interactions are considered, there are a limited number of conformations that create a reasonable bridge along the phosphate ester chain. The torsional angles of the linker were adjusted to closely match the spacing between phosphate groups. Since these bridging groups replace a single base along the DNA helix, they were then "docked" to the DNA helix and the base removed. After inserting both dye bridges, R and κ^2 were computed from the coordinates of Cy3 and Cy5 in CCDC Mercury (version 3.1.1), Supporting Information Figure S1. Here, κ^2 is calculated using

$$\kappa^2 = (\hat{a}\cdot\hat{d} - 3(\hat{a}\cdot\hat{r})(\hat{r}\cdot\hat{d}))^2 \quad (5)$$

where $\hat{a}$ and $\hat{d}$ are the unit vectors of the acceptor and donor transition dipole moments, represented here for each molecule by the vector that points from one end of the molecule to the other end. $\hat{r}$ is the unit vector that connects the center of the two transition dipoles, represented here by the vector connecting the center of the two molecules. This representation implies that the absorption and emission dipoles of the cyanines aligned, which is supported by transient fluorescence anisotropy measurements.[18]

Steady State Spectroscopy. Steady state absorption spectra were measured using an Agilent UV−Vis Chemstation. Steady state ensemble fluorescence spectra and fluorescence excitation profiles (FEP), i.e., photoluminescence excitation spectra, corrected for instrumental effects were taken on a dual monochromator multifunction microtiter plate reader (Tecan Safire).

Fluorescence quantum yields were measured on samples with peak optical densities < 0.1. The fluorescence intensity was referenced to rhodamine B in ethanol, which was measured to have a quantum yield of 0.68 when referenced to rhodamine 6G in agreement with literature values.[24]

RET can be quantified through steady state fluorescence measurements. RET leads to simultaneous quenching of the donor emission and sensitization of the acceptor emission. The RET efficiency can be calculated from donor quenching measurements by[5]

$$E_F = 1 - \frac{F_{DA}}{F_D} \quad (6)$$

where F_{DA} and F_D are the donor peak fluorescence intensities of the two-dye-labeled DNA duplex and the Cy3-only-labeled control duplex, respectively.

Single-Pair FRET. spFRET experiments were carried out using an Axiovert inverted microscope (Zeiss). Laser excitation was obtained using the 515 nm line of an argon ion laser that was coupled into a single-mode optical fiber. The output from the fiber was then tightly focused into the sample solution using

dx.doi.org/10.1021/jp5065006 | J. Phys. Chem. B 2014, 118, 14555−14565

a 100× neofluar objective (1.4× N.A., Zeiss). The DNA duplexes were placed in individual sample wells of an eight-well sample tray (Thermo-Scientific) at a concentration of 30−50 pM in 2.5 × PBS. The freely diffusing single-DNA structures were excited as they passed through the laser focus. To reduce photobleaching of the dyes, an oxygen scavenging system was used consisting of 4 mg/mL glucose, 2 mM trolox (Sigma-Aldrich), 1 mg/mL glucose oxidase (Sigma-Aldrich), and 0.04 mg/mL catalase (Sigma-Aldrich).[25] The fluorescence from the samples was focused onto a 75 μm pinhole to reject the out-of-focus emission. After the pinhole, the Cy3 and Cy5 fluorescence was separated using a dichroic filter (FF640-Di01, Semrock) and then detected using a single-photon avalanche detector (SPCM-ARQH-14, Excelitas) in each channel. The fluorescence burst signal from each detector was collected using a counter/timer board (PCI-6602, National Instruments). The laser power was adjusted to give a maximum burst level of about 100 counts, which corresponded to an optical power of less than 75 μW before the objective. The signals from each channel were processed into RET efficiency histograms using custom-designed software following the method of Pons et al.[12] An event was counted when the sum burst signals from both channels exceeded a threshold of 30 counts. The energy transfer efficiency from spFRET is determined from

$$E_{\mathrm{spFRET}} = \frac{I_{\mathrm{Cy5}}}{I_{\mathrm{Cy5}} + \gamma I_{\mathrm{Cy3}}} \tag{7}$$

where I_{Cy3} and I_{Cy5} are the photon burst signals in the Cy3 and Cy5 channels, respectively. The factor γ is related to the fluorescent quantum yields of the dyes and the detection efficiencies of the two channels.[11] The γ factor was adjusted for variations in the Cy3 fluorescence quantum yield, as given in Table 1.

Time-Resolved Fluorescence. The Cy3 and Cy5 fluorescence dynamics were measured via the time-correlated single photon counting (TCSPC) technique using a Becker-Hickl SPC-630 board. The system was based on a 80 MHz 7 ps pulsed 532 nm frequency-doubled diode-pumped Nd:YVO_4 laser (High-Q picoTRAIN). DNA duplexes in 2.5 × PBS buffer/water solutions (~1 μM) were placed in 1 mm path quartz spectrophotometric cells. The sample fluorescence was sent through a polarizer set to the magic angle[26] and then filtered using a monochromator. We then used a microchannel plate photomultiplier tube (Hamamatsu) to detect the fluorescence. A ~45 ps instrument response function (IRF) was measured using scattered light from a scattering solution in the fluorescence cell.

Ultrafast Spectroscopy. Two-color pump−probe spectroscopy was used to examine excited state and ET dynamics in the DNA duplexes. The experimental setup is described elsewhere.[27] In brief, it was based upon a Ti:sapphire amplifier (CPA2101, Clark-MXR), which was used to pump two optical parametric amplifiers (OPAs). A noncollinear visible OPA was used to produce the pump, while a frequency-doubled infrared OPA produced the probe. Balanced Si photodiodes and a preamplifer were used to suppress noise. Lock-in detection of the ground state bleach (GSB) or stimulated emission (SE) was used to measure the RET dynamics, which are reported in terms of the delay-dependent normalized change in transmission ($\Delta T/T_0$). DNA duplexes in 2.5 × PBS buffer/water solutions (~1 μM) were placed in 1 cm path cuvettes, maintained at 10 °C using a cooling block connected to a water circulator and stirred at 100 rpm throughout illumination to suppress photodegradation or thermal degradation. The pump−probe IRF that was measured via two-photon absorption in ZnSe was 400 fs, which is much faster than that available through TCSPC. A 150 mm delay stage allows for measurements up to a maximum pump−probe delay of 1 ns.

Transient absorption (TA) spectroscopy was used to identify the GSB and SE bands. In this case, a white light probe beam is derived from self-phase modulation by focusing 775 nm light into a 1 mm thick sapphire plate and used to probe the photoexcited DNA duplexes. After traversing the sample, the white light probe is sent through a scanning monochromator (SPEX 270M) and into a Si photodiode.

For measurements of RET dynamics, DNA duplexes labeled with the Cy3 donor were photoexcited near the absorption peak at 553 nm. The Cy3 SE band was probed at 565 nm for both donor-only-labeled (i.e., control samples) and donor−acceptor-labeled duplexes. Duplexes containing the Cy5 acceptor alone (i.e., control samples) were photoexcited at 610 nm. The Cy5 GSB and SE bands were probed at 650 and 675 nm respectively for both acceptor-only- and donor−acceptor-labeled DNA. The pump polarization was set at magic angle[26] with respect to the probe via a waveplate−polarizer pair to avoid possible transient effects associated with dye reorientation over our temporal window.

RET dynamics are typically characterized by a shortened donor excited state lifetime and a concomitant induction of the acceptor excited state.[28] Here we measure both the donor and acceptor excited state dynamics and account for the possibility of lone donors (e.g., in our case from unhybridized oligos containing Cy3 or from DNA duplexes containing dark Cy5) as well as direct excitation of acceptors. For a homogeneous system, the RET dynamics can be described by a simple two-state model where we consider the RET rate as well as the donor and acceptor excited state decay rates, k_{D} and k_{A}, respectively. Solving the rate equations for the donor ($D(t)$) and acceptor dynamics ($A(t)$) yields

$$D(t) = D_0 e^{-(k_{\mathrm{D}}+k_{\mathrm{RET}})t}$$

$$A(t) = \frac{D_0 k_{\mathrm{RET}}}{k_{\mathrm{A}} - (k_{\mathrm{D}} + k_{\mathrm{RET}})}\left[e^{-(k_{\mathrm{D}}+k_{\mathrm{RET}})t} - e^{-k_{\mathrm{A}}t}\right] \tag{8}$$

where D_0 is the initial concentration of donor species and k_{RET} is the rate constant for energy transfer from donor to acceptor. The presence of lone donors leads to a subpopulation of donors that exhibit the typical donor lifetime unaffected by RET. The presence of directly photoexcited acceptors leads to a subpopulation of acceptors with a near-instantaneous response and the typical acceptor decay dynamics.[29] Any intrinsic rise time, $(k_{\mathrm{A,rise}})^{-1}$, to the acceptor excited state should also be included. This allows for accurate estimation of the RET rate while properly accounting for lone donors and directly excited acceptor molecules.

RESULTS AND DISCUSSION

Steady State Spectroscopy. The estimation of the Förster radius via eq 3 requires determination of the Cy3 fluorescence quantum yield, Q_{D}, and calculation of the Cy3−Cy5 overlap integral. Typical absorption and emission spectra of DNA duplexes containing only Cy3 or Cy5 are shown in Figure 1b. Similar to recent reports in literature,[10] we observe changes in

dx.doi.org/10.1021/jp5065006 | J. Phys. Chem. B 2014, 118, 14555−14565

Table 1. Comparison between Structural Model, Fluorescence, and spFRET Measurements

			calculated from structural model					fluorescence	spFRET
N	Q_D (%)[a]	τ_D (ps)	R (Å)	κ^2	R_0 (Å)[b]	E[c]	k_{RET}^{-1} (ps)	E_F[d]	E_{spFRET}
0	26 ± 2	1169 ± 9	28.3	0.93	62.3 ± 0.9	0.99	10.2 ± 0.9	0.97	0.96 ± 0.01
1	26 ± 2	1290 ± 10	30.2	0.69	59.4 ± 0.8	0.98	22 ± 2	0.95	0.95 ± 0.01
2	27 ± 2	1252 ± 7	29.8	0.38	54.0 ± 0.7	0.97	36 ± 3	0.91	0.93 ± 0.02
3	26 ± 2	1126 ± 7	27.6	0.08	41.0 ± 0.6	0.92	104 ± 9	0.94	0.94 ± 0.02
4	30 ± 2	1172 ± 7	24.2	0.09	43.7 ± 0.8	0.97	34 ± 4	0.87	0.94 ± 0.02
5	32 ± 3	1300 ± 10	21.3	1.45	70 ± 1	0.99	1.1 ± 0.1	0.91	0.94 ± 0.02
6	39 ± 4	1620 ± 20	21.2	3.48	83 ± 1	0.99	0.44 ± 0.05	0.92	0.92 ± 0.02
7	29 ± 3	1290 ± 10	24.8	2.85	77 ± 1	0.99	1.5 ± 0.2	0.86	0.88 ± 0.02
8	26 ± 2	990 ± 10	30.7	1.57	68 ± 1	0.99	8.3 ± 0.7	0.86	0.84 ± 0.02
9	22 ± 2	802 ± 8	37.2	1.00	61 ± 1	0.95	40 ± 4	0.82	0.81 ± 0.02
10	34 ± 3	1460 ± 20	43.1	0.87	65 ± 1	0.92	130 ± 20	0.77	0.77 ± 0.02
11	30 ± 2	1240 ± 20	47.5	1.02	65 ± 1	0.87	190 ± 20	0.67	0.70 ± 0.02
12	30 ± 2	1352 ± 8	50.5	1.39	68 ± 1	0.86	230 ± 30	0.60	0.67 ± 0.02
13	21 ± 1	880 ± 20	52.1	1.96	68.1 ± 0.7	0.83	170 ± 10	0.46	0.52 ± 0.02
14	19 ± 1	890 ± 20	52.8	2.68	70.6 ± 0.7	0.85	160 ± 10	0.44	0.48 ± 0.02
15	18 ± 1	960 ± 20	53.5	3.39	72.8 ± 0.8	0.86	150 ± 10	0.43	0.44 ± 0.02
16	33 ± 3	1416 ± 9	55.1	3.78	82 ± 1	0.92	130 ± 10	-	0.42 ± 0.02

[a]Uncertainty represented by standard deviation from multiple measurements. [b]$J(\lambda)$ was taken as 8.7×10^{13} cm^3·M^{-1}; propagated uncertainty from Q_D only. [c]Propagated uncertainties from Q_D is typically <1%. [d]Uncertainty is typically ~5%.

the donor fluorescence quantum yield due to changes in the local environment as the Cy3 position was varied, Table 1. We can, however, treat the Cy5 optical properties as constant, since its position on the DNA duplex was not varied. The average overlap integral was 8.7×10^{-13} cm^{-3}·M^{-1}, which agrees with the literature.[5,30] The average calculated R_0, assuming $\kappa^2 = 2/3$, was 59 ± 2 Å.

The absorption spectra of the two-dye-labeled DNA duplexes were also examined. For $N > 3$ base pairs, the Cy3 absorption bands have similar shape and we conclude that they are unperturbed by Cy5. Significant changes in the Cy3 absorption band shape result for Cy3 and Cy5 attachment points corresponding to $N < 4$ base pairs, Supporting Information Figure S2. The Cy3 absorption maximum progressively shifts to the blue. The largest blue shift of ~12 nm occurs for the $N = 0$ case, Figure 2. Further, the absorption shoulder near 518 nm progressively broadens. The hypsochromic shift suggests excitonic coupling due to H-type heterodimers of Cy3 and Cy5. In contrast, the Cy5 absorption band shows relatively little dependence on the Cy3−Cy5 separation. FEPs (not shown) were measured in the Cy3 region while collecting the fluorescence emitted in the Cy5 region near 700 nm. The FEPs show qualitatively similar dependence on base-pair separation as the absorption spectra, which is not expected if H-dimer formation is dominant. The similarity of the absorption and FEP suggest that Cy3−Cy5 interactions do not produce significant concentrations of strict J-like or H-like dimers that would result in strongly distorted Cy3 and Cy5 absorption bands.[31] For DNA duplexes with closely spaced Cy3 and Cy5 ($N < 4$) we conclude that we may still consider the Cy3 and Cy5 as approximately distinct donor−acceptor pairs, though not satisfying the weak-coupling limit assumed by Förster theory where the absorption bands of the donor−acceptor pair are unperturbed. The Cy3−Cy5 coupling is discussed further later in the context of evaluating the structural model and measured RET rates.

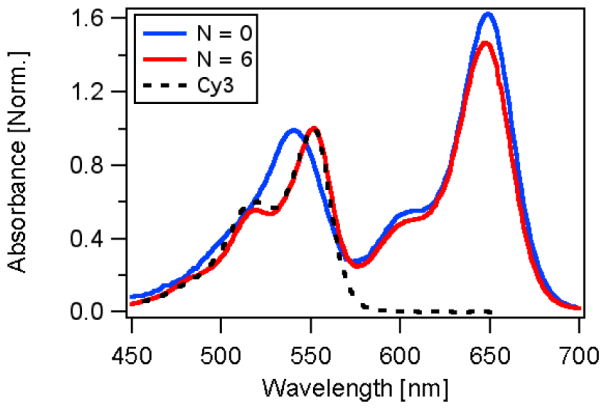

Figure 2. Absorption spectra for Cy3−Cy5 pairs corresponding to $N = 0$ (blue) and $N = 6$ (red), and a control containing Cy3 only (black, dashed).

The Cy5 fluorescence quantum yield, Q_A, was measured to be 0.28 for Cy5-only-labeled DNA duplexes. This is expected, as the local environment for Cy5 remains the same for all of the duplexes. For $N > 3$, the Cy3−Cy5 DNA show the same Q_A. However, for $N < 4$ we observe a decrease in the Cy5 quantum yield. For $N = 0$, $Q_A = 0.10$. When in close proximity, the interaction between Cy3 and Cy5 partially quenches the Cy5 emission. This is discussed further later in the context of time-resolved measurements.

Steady state fluorescence spectra of the two-dye-labeled DNA duplexes were measured. The Cy3-only-labeled controls were also measured for each case. Figure 3a shows fluorescence spectra of a subset of two-dye-labeled duplexes for $N = 0$, 6, 8, and 11, and a typical reference spectrum for Cy3 (the $N = 8$ control). For each case, the fluorescence peaks and band shapes are nearly the same. The relatively low intensity of the Cy5 emission band for $N = 0$ is likely due to partial quenching from interaction with the Cy3 dye. Further evidence for this conclusion is found from time-resolved measurements, which are discussed below. The inset to Figure 3a shows the RET efficiencies, see Table 1, calculated from the observed donor quenching using eq 6. The RET efficiency (E_F) increases from 43% to 97% as N decreases from 15 to 0 base pairs. For $N = 16$,

dx.doi.org/10.1021/jp5065006 | J. Phys. Chem. B 2014, 118, 14555−14565

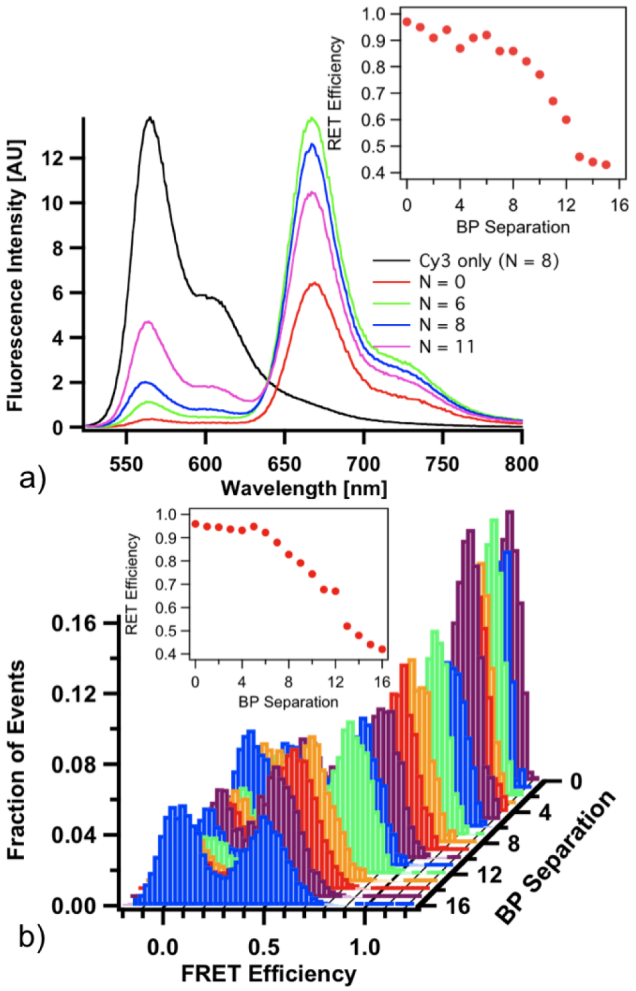

Figure 3. (a) Fluorescence spectra of Cy3, and the N = 0, 6, 8, and 11 two-dye-labeled DNA duplexes. The inset shows the efficiency calculated from the donor sensitization using eq 6. (b) spFRET energy transfer efficiency histograms for N = 0−16 base-pair separation. The inset shows the efficiency resulting from a Gaussian fit to the high efficiency peak.

formation errors led to excess Cy3, which made it impractical to estimate the RET efficiency from donor quenching. The observation that the RET efficiency falls slightly short of 100% at close Cy3−Cy5 separations may be related to the presence of unhybridized oligos. A static distribution of dye−dye orientations would also lead to less than 100% RET for close Cy3−Cy5 separations.[32]

Single-Pair FRET. To further quantify energy transfer efficiency and to check for subpopulations, spFRET measurements were performed on the DNA duplex series, Figure 3b. We note that the γ factor used in eq 7 ignores the changes in Q_A and potential changes in Q_D due to dye interaction for the closest base-pair separations (N < 4). Histograms of the distribution of RET efficiencies were generated for each sample and fit with Gaussian distributions. A single distribution of high RET efficiency was observed for all samples, Supporting Information Figure S3. Thus, if distinct high RET subpopulations exist, they are not resolvable within the experimental configuration. For each sample a second distribution near zero RET was also present, which may be caused by unhybridized oligos or photobleached dye-labeled DNA.

The RET efficiencies (E_{spFRET}) are qualitatively similar to those determined from the ensemble donor quenching measurements (E_F), though there is less scatter in the N dependence. We observe that the RET efficiency increases from 42% to 96% as N decreases. As expected the RET efficiency saturates for small N; however, it does not reach 100%. In the context of our structural model, geometric considerations tell us that for N = 0 we should expect $R \sim 28$ Å (see Table 1), which should result in an energy transfer efficiency near 99%. It is possible that inactive, i.e., nonemissive, or photobleached Cy5 dyes artificially decrease the measured RET efficiency. We also observe partial quenching of the Cy5 fluorescence for N < 4 as characterized by reduced fluorescence lifetimes and quantum yields, which would lead to underestimated RET efficiencies.

Time-Resolved Fluorescence. The fluorescence dynamics of Cy3-only-labeled (control) DNA duplexes varied for all constructs, consistent with the quantum yield measurements. The Cy3-only fluorescence decay curves are shown in Supporting Information Figure S4. In each case, the Cy3 dye is attached at a different position on the DNA duplex. The observed variation in Cy3 lifetime is consistent with recent reports that the fluorescence lifetimes of cyanine dyes attached via double phosphoramidite linkers depend on the local DNA sequence,[10] as well as reports that the fluorescence of cyanine dyes attached to the 5′ terminus of single-stranded DNA depends on the DNA sequence.[33] This may mean that the cyanine dyes are able to undergo trans (bright)−cis (dark) isomerization.[10] Though the dyes are not completely rigid, the relatively long observed lifetime, compared to free Cy3,[34] suggests that the double phosphoramidite attachment places some restriction on the torsional motion about the polymethine group. The Cy5 fluorescence lifetime remained unchanged, τ_A = 1.5 ns, for all DNA duplexes.

For the two-dye-labeled DNA duplexes we observed a decay in the Cy3 fluorescence and a concomitant induction in Cy5 fluorescence, Supporting Information Figure S5, which is consistent with RET. The specific case of N = 11 is shown in Figure 4a. The Cy3 excited state is depleted through energy transfer to Cy5, which in turns populates the Cy5 excited state. Due to rapid picosecond time scale RET, the TCSPC IRF limited our examination to the N = 8−16 DNA duplexes. Both the Cy3 decay and Cy5 induction dynamics were multiexponential. In particular, there were contributions from lone donors as well as two RET rates, from which we computed an amplitude-averaged RET rate found in Table 2. We observe a monotonic increase in the RET rate as the base-pair separation between Cy3 and Cy5 decreased, Figure 5. The corresponding RET efficiencies (E_{TR} in Table 2) are ∼1−15% higher than those found through spFRET measurements.

As a direct measurement of the RET rate, time-resolved spectroscopy can be a more accurate estimate of the RET efficiency than steady state methods. Here, subtle changes in the donor or acceptor emission dynamics can be directly linked to changes in the RET efficiency. On the other hand, steady state methods depend on the ratio of emission intensities, from which we can only indirectly infer information about RET and are therefore more susceptible to artifacts.

Ultrafast Spectroscopy. The GSB and SE dynamics of Cy5 alone (control) are similar for all constructs, which is consistent with similar observations for TCSPC and Q_A measurements. The GSB shows an instrument-limited rise followed by a ∼30 ps decay and a ∼1.5 ns decay. The SE shows a similar instrument-limited rise, followed by a ∼30 ps

dx.doi.org/10.1021/jp5065006 | J. Phys. Chem. B 2014, 118, 14555−14565

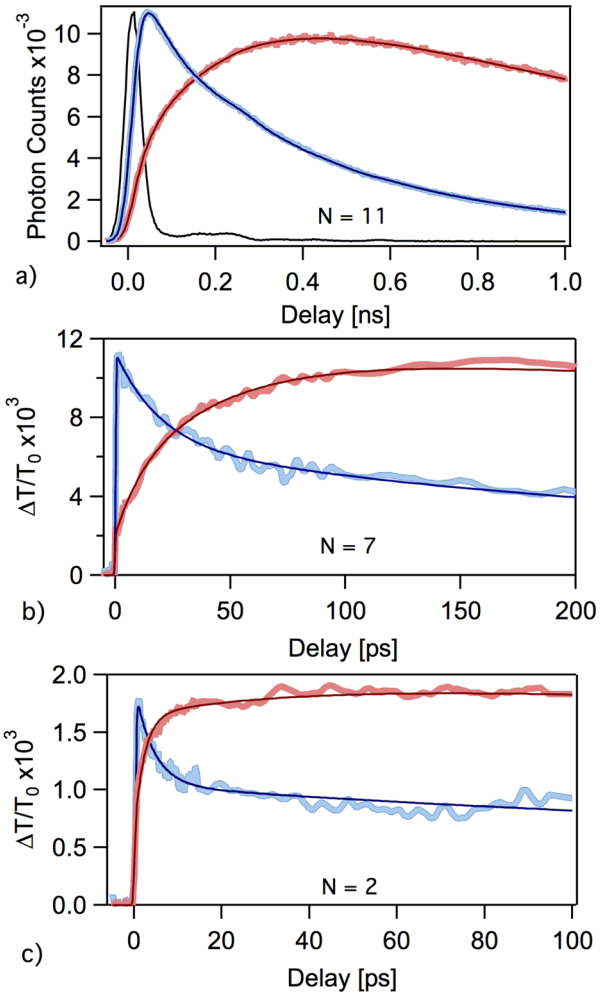

Figure 4. Representative Cy3 (blue) and Cy5 (red) excited state dynamics for the DNA duplexes measured via (a) TCSPC for $N = 11$ and ultrafast pump−probe spectroscopy for (b) $N = 7$ and (c) $N = 2$. Note the different time scales in each example. The black curve in (a) is the TCSPC instrument response.

induction that is complementary to the GSB decay, and a ∼1.5 ns decay that matches that seen for the GSB. TA spectra show that the Cy5 GSB and SE form one indistinguishable band that displays a red shift over the first 30 ps consistent with the pump−probe dynamics observations, Supporting Information Figure S6. Because these dynamics are too slow to be vibrational cooling within the excited state manifold, they are instead tentatively assigned to solvent reorganization around the excited state geometry.

Fast RET rates necessitated ultrafast pump−probe measurements of the excited state dynamics in the $N = 0$−7 DNA duplexes. Similar to observations from the TCSPC measurements, we observe a decay component in Cy3 SE and a complementary induction in Cy5 SE, Supporting Information Figure S5, which is consistent with RET. The specific cases of $N = 7$ and 2 are shown in Figure 4. Again we observe multiple RET rates for most DNA duplexes. The Cy3 and Cy5 SE dynamics are fit with a modified version of eq 8 that includes a second RET rate.[35] The fit results are collected in Table 2. Similarly, multiple RET rates have been observed in dynamics of donor and acceptor molecules in micelles.[29] Interestingly, spFRET measurements do not show a bimodal distribution of efficiencies despite similar amplitude weighting for each measured RET rate. Though Cy3 alone has multiexponential decay dynamics, k_{D1}^{-1} (1.96 ns) and k_{D2}^{-1} (560 ps), these rates do not differ sufficiently to produce the two observed RET rates. Given the double attachment of the dyes to the DNA backbone by short linkers, it is unlikely that this difference can be accounted for by a distribution of R[32,36] or by two different geometries.[15,37] Literature reports of large ($r \sim 0.3$) and slowly decaying anisotropy[18] shows that dye motion is restricted by the double phosphoramidite linkage and suggests that our system can be considered static on picosecond time scales. However, orientational heterogeneity may yield a distribution in κ^2. Because there are many ways to achieve $\kappa^2 = 0$, but relatively few favorable orientations, it is common to observe multiexponential decay dynamics that point to subpopulations that experience inefficient RET.[38] However, a clear picosecond-scale decay component is present, namely, k_{RET1}^{-1}. Transient absorption experiments, Supporting Information Figure S7, show that the excited state spectra of the DNA duplexes are a linear combination of the features associated with Cy3 and Cy5, with no evidence of charge transfer. A photoinduced absorption band of Cy5 overwhelms the Cy3 SE near 565 nm for the $N = 0$ DNA duplex, so the Cy3 SE was measured at 550 nm.

As the base-pair separation between the donor and acceptor becomes smaller, the Cy5 SE becomes stronger and exhibits a faster rise, which is consistent with the expected increase in RET efficiency and rate, Supporting Information Figure S5. For $N = 0$ the Cy5 SE rise is instrument-limited. Unexpectedly, the Cy5 SE decay becomes faster for $N < 4$, Supporting Information Figure S8. However, this is consistent with the reduced Q_A observed in these duplexes. The interaction between Cy3 and Cy5 leads to partial quenching of the Cy5 emission. Similar partial quenching due to dye interaction has been observed in fluorescence dynamics[39] and single-particle measurements[40] of rhodamine derivatives attached to DNA duplexes via flexible linkers. Both studies found that Cy3−Cy5 exhibited comparatively little interaction for $N \geq 6$.

In the distance regime where $R < R_0/2$, the RET rate is a more sensitive measurement of donor−acceptor separation distance than RET efficiency. This arises from the saturation of the RET efficiency as it asymptotically approaches unity for small donor−acceptor separations. Currently available RET efficiency measurements lack sufficient precision to discern small deviations from 100% RET. Over these same distances the RET rate changes dramatically, varying by orders of magnitude. For the short Cy3−Cy5 separation distances studied here, ultrafast spectroscopy provides a more precise measurement of the agreement with Förster theory.

The structural model shown in Figure 1 of dye position and orientation as a function N was used to evaluate the level of agreement between our measurements and Förster theory. We begin with the assumption that the dyes are attached rigidly and held outside the DNA backbone, as shown in Figure 1. For rigidly attached dyes, we expect that R and κ^2 will be correlated.[41] The resulting R and κ^2, which are found using the scheme described in Supporting Information Figure S1, and estimated RET efficiencies from our structural models are given in Table 1.

We do not observe good agreement between the RET efficiencies estimated by applying Förster theory to our structural model (E) and the RET efficiencies derived from our time-resolved measurements (E_{TR}), Figure 5a. This disagreement seems to stem from the calculated values of κ^2, which predict favorable orientations for RET for $N > 11$ bp.

dx.doi.org/10.1021/jp5065006 | J. Phys. Chem. B 2014, 118, 14555−14565

Table 2. Fit Parameters to the Time-Resolved Fluorescence and Ultrafast Spectroscopy Dynamics

	calculated from Cy3 dynamics				calculated from Cy5 dynamics				average	
N	A_1	k_{RET1}^{-1} (ps)	A_2	k_{RET2}^{-1} (ps)	A_1	k_{RET1}^{-1} (ps)	A_2	k_{RET2}^{-1} (ps)	k_{RET}^{-1} (ps)[a]	E_{TR}[b]
0	110	2.9 ± 0.4	65	51 ± 8		0.4 ± 0.1			11 ± 2	0.99
1	102	3.6 ± 0.2	83	120 ± 20		1.2 ± 0.1			29 ± 5	0.98
2	81	4.2 ± 0.2	35	150 ± 20		2.3 ± 0.1			25 ± 3	0.98
3	40	1.4 ± 0.2	29	37 ± 3		2.6 ± 0.1			9.5 ± 0.7	0.99
4	430	3.5 ± 0.2	309	78 ± 5	63	2.1 ± 0.3	82	26 ± 1	25 ± 1	0.98
5	171	7.9 ± 0.5	134	270 ± 40	72	3.5 ± 0.3	83	37 ± 2	73 ± 9	0.95
6	347	7.3 ± 0.5	312	220 ± 20	104	7.4 ± 0.5	138	67 ± 3	75 ± 5	0.96
7	465	20 ± 1	387	270 ± 20	59	11 ± 1	164	46 ± 3	85 ± 5	0.94
8	1376	56 ± 2	802	324 ± 5	644	14 ± 2	821	95 ± 6	100 ± 3	0.91
9	1111	68 ± 2	700	540 ± 10	673	28 ± 3	632	151 ± 8	144 ± 3	0.85
10	3230	93 ± 1	2261	480 ± 4	546	41 ± 4	965	175 ± 6	178 ± 3	0.89
11	2512	140 ± 2	2316	664 ± 8	261	51 ± 8	893	250 ± 7	275 ± 4	0.82
12	557	162 ± 6	825	910 ± 10	221	63 ± 9	848	376 ± 8	418 ± 6	0.77
13	713	182 ± 9	1669	1190 ± 30		414 ± 9			573 ± 9	0.61
14	361	190 ± 13	939	1110 ± 40		450 ± 10			590 ± 10	0.61
15	309	210 ± 20	1015	1120 ± 30		540 ± 10			670 ± 10	0.59
16		1030 ± 20				657 ± 9			840 ± 10	0.63

[a] k_{RET}^{-1} is the mean of the two amplitude weighted averages of k_{RET1}^{-1} and k_{RET2}^{-1} from the Cy3 and Cy5 dynamics. The propagated uncertainties are based on uncertainties in fit parameters only. [b] E_{TR} is calculated from k_{RET}^{-1} using eqs 1 and 2; τ_D is given in Table 1.

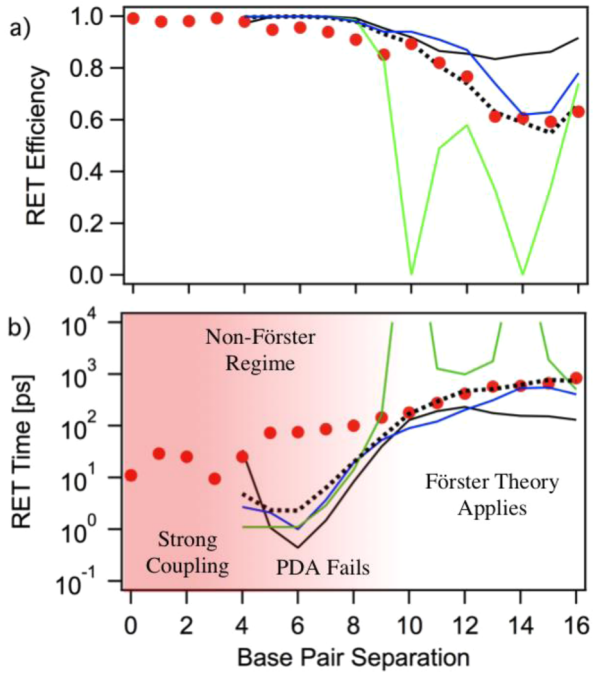

Figure 5. Measured (red dots) RET efficiency (a) and RET time (b) as a function of base-pair separation. Results calculated from the structural model (black), intercalation model (green), and a model that averages the rates from each of the four combinations of the structural and intercalated models (blue) are shown for comparison. The dashed line is calculated from the structural model distances while assuming $\kappa^2 = 2/3$. The shaded area represents the dye separations where the assumptions of Förster theory begin to fail.

Evaluation of rigid and flexible linkers has found that rigid linkers can result in large errors in κ^2 that may outweigh the increased certainty in R.[42] If instead we assume $\kappa^2 = 2/3$, we observe good agreement between our structural model and measured RET efficiencies for $N \geq 10$. This agreement is surprising and is in conflict with the physical picture of dyes held rigidly by the double phosphoramidite attachment. The assumption that $\kappa^2 = 2/3$ implies a dynamic average over an isotropic distribution of orientations, i.e., that the dyes are able to randomize their orientations on a shorter time scale than RET. However, anisotropy measurements of Cy3 attached to a DNA duplex via the double phosphoramidite linkage show that the dyes are not able to reorient for several nanoseconds.[18] Further, the dynamic average limit implies single-exponential RET dynamics, which is also in conflict with our observed multiexponential dynamics. Thus, we conclude that our results are better interpreted by considering a distribution of dipole orientations that are static over the RET time scale. Distributions of static dipoles can yield an average of $\kappa^2 = 2/3$ without sampling all possible orientations uniformly.[32] A static distribution of dipole orientations can also lead to acceptor induction that is consistently faster than the donor decay because the coefficients in eq 8 suppress slow RET rates contributing to the acceptor dynamics, which is consistent with the fit results in Table 2.

We first consider the case of a static isotropic distribution of dye orientations. Recent Monte Carlo simulations show that a static average over an isotropic distribution of orientations yields bimodal distributions of RET efficiencies,[32] with the largest distribution near zero due to the larger number of possible unfavorable orientations. A comparison between those simulations and our data shows pronounced disagreement for both spFRET efficiencies and RET dynamics; see the Supporting Information for details. Specifically, we find good agreement with our measured dynamics only if we consider an unphysically large Gaussian distribution of dye separations in addition to a static isotropic distribution of dipoles, Supporting Information Figure S10. Thus, we conclude that it is unlikely that the distribution of κ^2 is isotropic.

Very recently, it was suggested that cyanine dyes attached to DNA duplexes via double phosphoramidite linkers may intercalate into the void created by the missing nucleobase.[10] Such a geometry will yield very different predictions than a structural model that places the dyes outside the DNA backbone. To explore the possibility of dye intercalation, we utilized a simple geometric model of dyes oriented parallel to

dx.doi.org/10.1021/jp5065006 | J. Phys. Chem. B 2014, 118, 14555−14565

the normal vector of a helical space curve to calculate R and κ^2; see the Supporting Information for details. This model showed poor agreement with our measured RET efficiencies, as did a similar model of dye groove-binding. We conclude that intercalation and groove-binding are not the most preferred dye orientations for these DNA duplexes.

A more physical picture is constructed by considering that both the nonintercalated and the intercalated dye arrangements contribute to the distribution of orientations suggested by our measurements. Indeed, the molecular dynamics simulations of ref 10 show a distribution of low energy configurations for Cy3 attached to dsDNA via double phosphoramidite linkers, which includes both intercalated and nonintercalated configurations.[10] If we average the RET rates corresponding to equal weightings of the four combinations of nonintercalated and intercalated geometries (see the Supporting Information for details), we arrive at predicted RET rates that are very similar to those found from our structural model with $\kappa^2 = 2/3$, Figure 5b. Even better agreement with our measurements is found when Monte Carlo methods are used to allow for distributions of dye angles about each of these four modes, Supporting Information Figure S12. This supports our supposition that our two-dye-labeled DNA duplexes are composed of a distribution of dye orientations, including intercalated and nonintercalated geometries, which are statically averaged during the time-resolved RET measurements. This physical model can be approximately described, for $N > 4$, by our structural model with $\kappa^2 = 2/3$. However, application of RET theory directly to the arrangements predicted by molecular dynamics simulations would yield better predictions.

We observe lower RET efficiencies for $3 < N < 10$ than what is predicted by the models shown in Figure 5b. This disagreement becomes pronounced if we instead compare the measured and predicted RET time (i.e., inverse rate), Figure 5b shaded region. This highlights the sensitivity of the RET rate to donor–acceptor separation distance. RET efficiencies, which are often used in RET analysis, underestimate deviations from model predictions for small dye separations.

A source of these disagreements may be our implicit assumption that Förster theory can describe the RET taking place in these DNA duplexes. We apply Förster theory when calculating the RET efficiencies and rates from the structural model. There are a number of reports that the familiar R^6 dependence predicted by Förster theory fails when fluorophores are in close proximity, resulting in weaker distance dependence.[37,43−45] The slower increase RET efficiency we observe for $N < 10$ suggests a weaker distance dependence than that described by Förster theory. Förster theory utilizes the point dipole approximation (PDA), which describes the transition dipole (or multipole) moment of the fluorophore as a point at the center of the molecule. It is more accurate to instead picture a transition density made up of numerous monopoles.[46] When in close proximity, the coupling between fluorophores is dominated by local interactions between the edges of these transition densities. If R is not much larger than the physical size of the fluorophores, which is the case here given that Cy3 is ∼14 Å and Cy5 is ∼16 Å down their long axis, then the PDA is a poor approximation to the actual transition densities.[47] This failure of the PDA is predicted to be worse for fluorophores with restricted motion, such as those examined here, because orientational averaging present in flexible structures helps to cancel these errors.[48] The measured RET times converge to those predicted by the structural model for $N \geq 10$. This is consistent with the PDA becoming a better approximation as the Cy3–Cy5 spacing becomes larger than 40 Å, in agreement with recent predictions.[48] The shaded region of Figure 5b highlights that for $N < 10$ the PDA is increasingly violated and overestimates the RET rate.

The DNA duplexes with $N < 4$ are more difficult to understand. The perturbations to the Cy3 absorption bands for $N < 4$ imply that the dyes may be much closer than the structural model suggests. For example, for $N = 0$ the structural model places Cy3 and Cy5 on nearly opposite sides of the DNA with a separation > 28 Å. However, the observed spectral shifts in the Cy3 absorption spectrum (Figure 2 and Supporting Information Figure S2) and partial quenching of Cy5 emission (Supporting Information Figure S8) indicates a level of coupling only possible when the dyes are in close proximity. An estimate of R can be obtained from the molecular exciton model.[49] Within the dipole–dipole approximation,

$$V_{\mathrm{dip-dip}} = \frac{1}{4\pi\varepsilon_0}\frac{\kappa\mu_{\mathrm{Cy3}}\mu_{\mathrm{Cy5}}}{n^2R^3} \tag{9}$$

where $V_{\mathrm{dip-dip}}$ is the dipole–dipole interaction energy, μ is the transition dipole moment (in debye) for each dye, and κ is the orientation factor. The separation R may be estimated from the observed shift of the Cy3 and Cy5 bands in the coupled spectrum relative to the unperturbed band positions of Cy3 and Cy5. For the case of a coupled two-level system,

$$\Delta E_{\mathrm{coup}} = \sqrt{(\Delta E_{\mathrm{monomer}})^2 + (4V_{\mathrm{dip-dip}})^2} \tag{10}$$

where ΔE_{coup} is the energy difference between the Cy3 and Cy5 absorption bands in the coupled Cy3–Cy5 spectrum and $\Delta E_{\mathrm{monomer}}$ is the energy difference between the unperturbed (monomer) Cy3 and Cy5 absorption bands. We used $\mu_{\mathrm{Cy3}} = 11.9$ D and $\mu_{\mathrm{Cy5}} = 14.1$ D based on integration over the extinction coefficients and set $\kappa = 0.82$ (corresponding to $\kappa^2 = 2/3$). For the case of $N = 0$, $\Delta E_{\mathrm{coup}} \approx 3110$ cm^{-1}, and $\Delta E_{\mathrm{monomer}} \approx 2693$ cm^{-1} (from the data in Figure 1), we find that $R = 8.2$ Å. This is much smaller than the 28.3 Å predicted by the structural model. Similar considerations yield $R = 9.2$, 10, and 9.8 Å for $N = 1$, 2, and 3, respectively.

Though the structural model is inaccurate for small N, we could estimate the energy transfer rate for $N < 4$ based on dye separations estimated by applying eqs 9 and 10 to the observed absorption band shifts. The energy transfer times predicted by Förster theory for $R \leq 10$ Å are orders of magnitude faster than our observations for $N < 4$. This disagreement is not unexpected as the observed excitonic coupling violates the assumption of weak coupling between the donor and acceptor. Förster theory does not apply in such cases. It is clear that Förster theory increasingly overestimates the energy transfer rate as the dye separation distance is reduced. This is not only due to failure of the PDA but also, for smaller dye separations, due to violation of the weak-coupling limit.

While the preceding estimate of R from the molecular exciton model is based on the dipole–dipole approximation, it points to the importance of molecular dynamics simulations. In our structural model the dyes are attached in a way that minimizes steric effects, which results in the dyes positioned outside the DNA double helix. However, molecular dynamics have shown that this orientation is one possible low energy configuration for the dye.[10] The observed spectral shifts suggest that neighboring voids left by the missing nucleobases allow the DNA helix to deform in such a way as to produce strong dye

dx.doi.org/10.1021/jp5065006 | J. Phys. Chem. B 2014, 118, 14555−14565

interaction. Importantly, such dye interaction may play a critical role in the efficient RET observed in natural systems.[50] Molecular dynamics have shown that dye intercalation is another low energy configuration for this system,[10] which could be favored when neighboring voids weaken the DNA helix. Attraction between the Cy3 donor and Cy5 acceptor may favor short separation distances between intercalated dyes. This highlights the value of molecular dynamics models,[37,41] which account for van der Waals interactions between the dyes, to more accurately estimate their relative positions.

CONCLUSION

In conclusion, we examined the donor−acceptor separation dependence of the RET efficiency and rate in Cy3- and Cy5-labeled DNA duplexes. Complementary Cy3 decays and Cy5 induction and single-pair fluorescence measurements confirm that resonance energy transfer is the dominant photophysical process. For close dye separations, time-resolved spectroscopic methods are found to produce more accurate RET rates than steady state methods. The RET rate is found to be a more precise measurement of the donor−acceptor separation than the RET efficiency. Our results support a picture of the double phosphoramidite dye attachment producing a distribution of orientations including intercalated and nonintercalated geometries. Deviations from the RET predicted by Förster theory point to the failure of the point dipole approximation for donor−acceptor separations < 10 base pairs or a center-to-center distance of less than or approximately equal to 40 Å. Interactions between the dyes are observed that alter their optical properties for separations of less than four base pairs, suggesting that the voids caused by the removed nuclobases allow the DNA to deform and the dyes to interact. Here, the weak-coupling limit of Förster theory no longer applies.

Our findings have relevance to the design of DNA-based light harvesting antennae and may be summarized a follows. (1) For the Cy3−Cy5 pair the energy transfer efficiency is >85% for donor−acceptor separations ≤ 10 base pairs, suggesting that relatively high energy transfer efficiency is achieved for distances < 45 Å. (2) The double phosphoramidite attachment effectively localizes the Cy3 and Cy5 fluorophores which suppresses unwanted aggregates (e.g., dimers) for donor−acceptor separations of greater than three base pairs. (3) When using the double phosphoramidite attachment, it is best to avoid placing the cyanine fluorophores at the same or adjacent base-pair positions (i.e., $N = 0, 1, 2$) where there is an increased possibility of aggregation and dimer formation.

ASSOCIATED CONTENT

Supporting Information

Calculation of κ^2 from the structural model, absorption spectra for $N = 0$−6 DNA duplexes, spFRET histograms for all DNA duplexes, fluorescence lifetimes of Cy3-only-labeled DNA duplexes (controls), time-resolved dynamics for all DNA duplexes, Cy5 intrinsic induction dynamics, DNA duplex excited state spectra, Cy5 partial quenching dynamics, Monte Carlo simulations of static isotropic dipoles, geometric models of dye intercalation, groove-binding, and the combinations of intercalated and nonintercalated geometries. This material is available free of charge via the Internet at http://pubs.acs.org.

AUTHOR INFORMATION

Corresponding Authors

*(P.D.C.) E-mail: paul.cunningham@nrl.navy.mil.

*(J.S.M.) E-mail: joseph.melinger@nrl.navy.mil.

Notes

The authors declare no competing financial interest.

ACKNOWLEDGMENTS

This work was supported by the Nanoscience Institute at the Naval Research Laboratory and the Office of Naval Research.

REFERENCES

(1) Beljonne, D.; Curutchet, C.; Scholes, G. D.; Silbey, R. J. Beyond Förster Resonance Energy Transfer in Biological and Nanoscale Systems. *J. Phys. Chem. B* **2009**, *113*, 6583−6599.

(2) Seeman, N. C. DNA in a material world. *Nature* **2003**, *421*, 427−431.

(3) Vyawahare, S.; Eyal, S.; Mathews, K. D.; Quake, S. R. Nanometer-Scale Fluorescence Resonance Optical Waveguides. *Nano Lett.* **2004**, *4*, 1035−1039.

(4) Heilemann, M.; Kasper, R.; Tinnefeld, P.; Sauer, M. Dissecting and Reducing the Heterogeneity of Excited-State Energy Transport in DNA-Based Photonic Wires. *J. Am. Chem. Soc.* **2006**, *128*, 16864−16875.

(5) Boeneman, K.; Prasuhn, D. E.; Blanco-Canosa, J. B.; Dawson, P. E.; Melinger, J. S.; Ancona, M.; Stewart, M. H.; Susumu, K.; Huston, A.; Medintz, I. L. Self-Assembled Quantum Dot-Sensitized Multivalent DNA Photonic Wires. *J. Am. Chem. Soc.* **2010**, *132*, 18177−18190.

(6) Hannestad, J. K.; Gerrard, S. R.; Brown, T.; Albinsson, B. Self-Assembled DNA-Based Fluorescence Waveguide with Selectable Output. *Small* **2011**, *7*, 3178−3185.

(7) Dutta, P. K.; Varghese, R.; Nangreave, J.; Lin, S.; Yan, H.; Liu, Y. DNA-Directed Artificial Light-Harvesting Antenna. *J. Am. Chem. Soc.* **2011**, *133*, 11985−11993.

(8) Özhalici-Ünal, H.; Armitage, B. A. Fluorescent DNA Nanotags Based on a Self-Assembled DNA Tetrahedron. *ACS Nano* **2009**, *3*, 425−433.

(9) Stein, I. H.; Steinhauer, C.; Tinnefeld, P. Single-Molecule Four-Color FREt Visualizes Energy-Tranfer Paths on DNA Origami. *J. Am. Chem. Soc.* **2011**, *133*, 4193−4195.

(10) Stennett, E. M. S.; Ma, N.; van der Vaart, A.; Levitus, M. Photophysical and Dynamical Properties of Doubly Linked Cy3-DNA constructs. *J. Phys. Chem. B* **2014**, *118*, 152−163.

(11) Deniz, A. A.; Dahan, M.; Grunwell, J. R.; Ha, T.; Faulhaber, A. E.; Chemla, D. S.; Weiss, S.; Schultz, P. G. Single-Pair Fluorescence Resonance Energy Rransfer on Freely Diffusing Molecules: Observation of Förster Distance Dependence and Subpopulations. *Proc. Natl. Acad. Sci. U. S. A.* **1999**, *96*, 3670−3675.

(12) Pons, T.; Medintz, I. L.; Wang, X.; English, D. S.; Mattoussi, H. Solution-Phase Single Quantum Dot Fluorescence Resonance Energy Transfer. *J. Am. Chem. Soc.* **2006**, *128*, 15324−15331.

(13) Schuler, B.; Lipman, E. A.; Eaton, W. A. Probing the Free-Energy Surface for Protein Folding with Single-Molecule Fluorescence Spectroscopy. *Nature* **2002**, *419*, 743−747.

(14) Kato, T.; Kashida, H.; Kishida, H.; Yada, H.; Okamoto, H.; Asanuma, H. Developement of a Robust Model System of FRET Using Base Surrogates Tethering Fluorophores for Strict Control of Their Position and Orientation within DNA Duplex. *J. Am. Chem. Soc.* **2013**, *135*, 741−750.

(15) Xu, Q.-H.; Wang, S.; Korystov, D.; Mikhailovsky, A.; Bazan, G. C.; Moses, D.; Heeger, A. The Fluorescence Resonance Energy Transfer Gate: A Time-resolved Study. *Proc. Natl. Acad. Sci. U. S. A.* **2005**, *102*, 530−535.

(16) Buckhout-White, S.; Ancona, M.; Oh, E.; Deschamps, J. R.; Stewart, M. H.; Blanco-Canosa, J. B.; Dawson, P.; Goldman, E. R.; Medintz, I. L. Multimodal Characterization of a Linear DNA-Based Nanostructure. *ACS Nano* **2012**, *6*, 1026−1043.

(17) Wang, X.; Seeman, N. C. Assembly and Characterization of 8-Arm and 12-Arm DNA Branched Junctions. *J. Am. Chem. Soc.* **2007**, *129*, 8169−8176.

(18) Ranjit, S.; Gurunathan, K.; Levitus, M. Photophysics of Backbone Fluorescent DNA Modifications: Reducing Uncertainties in FRET. *J. Phys. Chem. B* **2009**, *113*, 7861−7866.
(19) Haugland, R. P. *The Handbook: A Guide to Fluorescent Probes and Labeling Technologies*; Invitrogen: San Diego, 2005.
(20) Martin, T. G.; Dietza, H. Magnesium-Free Self-Assembly of Multi-layer DNA Objects. *Nat. Commun.* **2012**, *3*, No. 1103.
(21) Macke, T. J.; Case, D. A., Modeling Unusual Nucleic Acid Structures. In *Molecular Modeling of Nucleic Acids*; Leontes, N. B., Santa Lucia, J., Jr.,, Eds.; American Chemical Society: Washington, DC, USA, 1998; Vol. *682*, pp 379−393.
(22) Pettersen, E. F.; Goddard, T. D.; Huang, C. C.; Couch, G. S.; Greenblatt, D. M.; Meng, E. C.; Ferrin, T. E. UCSF Chimera—A Visualization System for Exploratory Research and Analysis. *J. Comput. Chem.* **2004**, *25*, 1605−1612.
(23) Wang, J.; Wang, W.; Kollman, P. A.; Case, D. A. Automatic Atom Type and Bond Type Perception in Molecular Mechanical Calculations. *J. Mol. Graphics and Modeling* **2006**, *25*, 247−260.
(24) Lopez Arbeloa, F.; Ruiz Ojeda, P.; Lopez Arbeloa, I. Flourescence Self-quenching of the Molecular Forms of Rhodamine B in Aqueous and Ethanolic Solutions. *J. Lumin.* **1989**, *44*, 105−112.
(25) Rasnik, I.; Mckinney, S. A.; Ha, T. Non-blinking and Long Lasting Single-Molecule Fluorescence Imaging. *Nat. Methods* **2006**, *3*, 891−893.
(26) Tao, T. Time-Dependent Fluorescence Depolarization and Brownian Rotational Diffusion Coefficients of Macromolecules. *Biopolymers* **1969**, *8*, 609−632.
(27) Cunningham, P. D.; Boercker, J. E.; Placencia, D.; Tischler, J. G. Anisotrpic Absorption in PbSe Nanorods. *ACS Nano* **2014**, *8*, 581−590.
(28) Morrison, L. E. Homogeneous Detection of Specific DNA Sequences by Fluorescence Quenching and Energy Transfer. *J. Fluoresc.* **1999**, *9*, 187−196.
(29) Mondal, S. K.; Ghosh, S.; Sahu, K.; Mandal, U.; Bhattacharyya, K. Ultrafast Fluorescence Resonance Energy Transfer in a Reverse Micelle: Excitation Wavelength Dependence. *J. Chem. Phys.* **2006**, *125*, No. 224710.
(30) Iqbal, A.; Arslan, S.; Okumus, B.; Wilson, T. J.; Giraud, G.; Norman, D. G.; Ha, T.; Lilley, D. M. J. Orientation Dependence in Fluorescent Energy Transfer Between Cy3 and Cy5 Terminally Attached to Double-stranded Nucleic Acids. *Proc. Natl. Acad. Sci. U. S. A.* **2008**, *105*, 11176−11181.
(31) Johansson, M. K.; Fidder, H.; Dick, D.; Cook, R. M. Intramolecular Dimers: A New Strategy to Fluorescence Quenching in Dual-Labeled Oligonucleotide Probes. *J. Am. Chem. Soc.* **2002**, *124*, 6950−6956.
(32) Vogel, S. S.; Nguyen, T. A.; van der Meer, B. W.; Blank, P. S. The Impact of Heterogeneity and Dark Acceptor States on FRET: Implications for Using Fluorescent Protein Donors and Acceptors. *PloS ONE* **2012**, *7*, No. e49593.
(33) Kretschy, N.; Somoza, M. M. Comparison fo the Sequence-Dependent Fluorescence of the Cyanine Dyes Cy3, Cy5, DyLight DY547 and DyLight DY647 on Single-Stranded DNA. *PloS ONE* **2014**, *9*, No. e85605.
(34) Sanborn, M. E.; Connolly, B. K.; Gurunathan, K.; Levitus, M. Fluorescence Properties and Photophysics of the Sulfoindocyanine Cy3 Linked Covalently to DNA. *J. Phys. Chem. B* **2007**, *111*, 11064−11074.
(35) Wegner, D.; Geibler, D.; Stufler, S.; Lohmannsroben, H.-G.; Hildebrandt, N. Time-resolved and Steady-state FRET Spectroscopy on Commercial Biocompatible Quantum Dots. *Proc. SPIE* **2011**, *7909*, 79090D.
(36) Hoefling, M.; Lima, N.; Haenni, D.; Seidel, C. A. M.; Schuler, B.; Grubmüller, H. Structural Heterogeneity and Quantitative FRET Efficiency Distributions of Polyprolines through a Hybrid Atomistic Simulation and Monte Carlo Approach. *PloS ONE* **2011**, *6*, No. e19791.
(37) Dolghih, E.; Roitberg, A. E.; Krause, J. L. Fluorescence Resonance Energy Transfer in Dye-labeled DNA. *J. Photochem. Photobiol., A* **2007**, *190*, 321−327.
(38) van der Meer, B. W.; van der Meer, D. M.; Vogel, S. S. Optimizing the Orientation Factor Kappa-Squared for More Accurate FRET Measurements. In *FRET—Förster Resonance Energy Transfer: From Theory to Applications*; Medintz, I. L., Hildebrandt, N., Eds.; Wiley-VCH: Weinheim, Germany, 2013.
(39) Dietrich, A.; Buschmann, V.; Muller, C.; Sauer, M. Fluorescence Resonance Energy Transfer (FRET) and Competing Processes in Donor-Acceptor Substituted DNA Strands: A Comparative Study of Ensemble and Single-Molecule Data. *Rev. Mol. Biotechnol.* **2002**, *82*, 211−231.
(40) DiFiori, N.; Meller, A. The Effect of Dye-Dye Interaction on the Spatial Resolution of Single Molecule FRET Measurements in Nucleic Acids. *Biophys. J.* **2010**, *98*, 2265−2272.
(41) VanBeek, D. B.; Zwier, M. C.; Shorb, J. M.; Krueger, B. P. Fretting about FRET: Correlation Between k and R. *Biophys. J.* **2007**, *92*, 4168−4178.
(42) Sindbert, S.; Kalinin, S.; Nguyen, H.; Kienzler, A.; Clima, L.; Bannwarth, W.; Appel, B.; Muller, S.; Seidel, C. A. M. Accurate Distance Determination of Nucleic Acids via Förster Resonance Energy Transfer: Implications of Dye Linker Length and Rigidity. *J. Am. Chem. Soc.* **2011**, *133*, 2463−2480.
(43) Schuler, B.; Lipman, E. A.; Steinbach, P. J.; Kumke, M.; Eaton, W. A. Polyproline and the "Spectroscopic Ruler" Revisited with Single-molecule Fluorescence. *Proc. Natl. Acad. Sci. U. S. A.* **2005**, *102*, 2754−2759.
(44) Saini, S.; Srinivas, G.; Bagchi, B. Distance and Orientation Dependence of Excitation Enery Transfer: From Molecular Systems to Metal Nanoparticles. *J. Phys. Chem. B* **2009**, *113*, 1817−1832.
(45) Wozniak, A. K.; Schröder, G. F.; Grubmüller, H.; Seidel, C. A. M.; Oesterhelt, F. Single-Molecule FRET Measures Bends and Kinks in DNA. *Proc. Natl. Acad. Sci. U. S. A.* **2008**, *105*, 18337−18342.
(46) Krueger, B. P.; Scholes, G. D.; Fleming, G. R. Calculation of Couplings and Energy-Transfer Pathways between the Pigments of LH2 by the ab Initio Transition Density Cube Method. *J. Phys. Chem. B* **1998**, *102*, 5378−5386.
(47) Speelman, A. L.; Muñoz-Losa, A.; Hinkle, K. L.; VanBeek, D. B.; Mennucci, B.; Krueger, B. P. Using Molecular Dynamics and Quantum Mechanics Calculations To Model Fluorescence Observables. *J. Phys. Chem. A* **2011**, *115*, 3997−4008.
(48) Munoz-Losa, A.; Curutchet, C.; Krueger, B. P.; Hartsell, L. R.; Mennucci, B. Fretting about FRET: Failure of the Ideal Dipole Approximation. *Biophys. J.* **2009**, *96*, 4779−4788.
(49) Kasha, M.; Rawls, H. R.; El-Bayoami, M. A. The Molecular Exciton Model in Molecular Spectroscopy. *Pure Appl. Chem.* **1965**, *11*, 371−392.
(50) Lee, H.; Cheng, Y.-C.; Fleming, G. R. Coherence Dynamics in Photosynthesis: Protein Protection of Exciton Coherence. *Science* **2007**, *316*, 1462−1465.